




The human *FOXM1* homolog promotes basal progenitor cell proliferation and cortical folding in mouse

Wenwen Wang^{1,2}, Libo Su^{2,3}, Fen Ji^{2,3}, Dongming Zhang^{2,3}, Yanyan Wang^{2,3}, Jinyue Zhao^{2,3}, Ross Dingyan Jiao⁴, Mengtian Zhang^{2,3}, Enyu Huang⁵, Hong Jiang^{6,*} , Jingjing Zhang^{5,**}  & Jianwei Jiao^{2,3,7,8,***} 

Abstract

Cortical expansion and folding are key processes in human brain development and evolution and are considered to be principal elements of intellectual ability. How cortical folding has evolved and is induced during embryo development is not well understood. Here, we show that the expression of human *FOXM1* promotes basal progenitor cell proliferation and induces cortical thickening and folding in mice. Human-specific protein sequences further promote the generation of basal progenitor cells. Human *FOXM1* increases the proliferation of neural progenitors by binding to the *Lin28a* promoter and increasing *Lin28a* expression. Furthermore, overexpression of *LIN28A* rescues the proliferation of human *FOXM1* knockout neural progenitor cells. Together, our findings demonstrate that a human gene can increase the number of basal progenitor cells in mice, leading to brain size increase and gyrfication, and may thus contribute to evolutionary brain development and cortical expansion.

Keywords brain development; cortical expansion; human *FOXM1*; *LIN28A*

Subject Categories Evolution & Ecology; Neuroscience

DOI 10.15252/embr.202153602 | Received 11 July 2021 | Revised 29 November 2021 | Accepted 13 December 2021 | Published online 22 December 2021

EMBO Reports (2022) 23: e53602

Introduction

During mammalian brain development and evolution, cortical expansion and gyrfication are considered a key hallmark, leading to

increased intellectual capacity (Chenn & Walsh, 2002; Lui *et al*, 2011; Zilles *et al*, 2013; Fernandez *et al*, 2016). The process is thought to reflect increasing numbers of cortical neurons, resulting from the increased proliferative ability of neural stem cells and neural progenitor cells during embryonic development (Sun & Hevner, 2014; Dehay *et al*, 2015).

Recently, some studies have shown that the outer subventricular zone (OSVZ) plays a key role in the cortical development of gyrencephalic species, such as humans and ferrets. The OSVZ contains basal radial glial cells and intermediate progenitors (Fietz *et al*, 2010). Basal radial glial cells (bRGs) are very abundant in gyrencephalic mammals such as ferrets and humans but rare in lissencephalic species such as rodents (Hansen *et al*, 2010; Reillo *et al*, 2011; Reillo & Borrell, 2012). The cellular and molecular mechanisms regulating the development of OSVZ and bRG have not been fully studied. Transcriptome sequencing and single-cell RNA sequencing have been used to study the cellular and molecular mechanisms of human neural progenitor cells (Fietz *et al*, 2012; Miller *et al*, 2014; Florio *et al*, 2018). Researchers have analyzed the difference fetal human ventricular zone (VZ), the inner subventricular zone (iSVZ), and outer subventricular zone (oSVZ), cortical plate and progenitor subpopulations using transcriptome sequencing, which showed that the human *FOXM1* gene is mainly distributed in proliferation-associated VZ, iSVZ, and oSVZ regions (Florio *et al*, 2015) and expressed in RG and IP (Pollen *et al*, 2015). Single cell RNA-seq datasets showed that the human *FOXM1* gene is enriched in basal RGCs (Liu *et al*, 2017; Dataset EV1). *FOXM1* is a typical proliferation-associated transcription factor, which is widely expressed in proliferating cells (Costa, 2005; Wierstra & Alves,

1 School of Life Sciences, University of Science and Technology of China, Hefei, China

2 State Key Laboratory of Stem Cell and Reproductive Biology, Institute of Zoology, Chinese Academy of Sciences, Beijing, China

3 University of Chinese Academy of Sciences, Beijing, China

4 Beijing Royal School, Beijing, China

5 Affiliated Hospital of Guangdong Medical University & Key Laboratory of Zebrafish Model for Development and Disease of Guangdong Medical University, Zhanjiang, China

6 Department of Physiology, Shandong Provincial Key Laboratory of Pathogenesis and Prevention of Neurological Disorders and State Key Disciplines: Physiology, School of Basic Medicine, Medical College, Qingdao University, Qingdao, China

7 Co-Innovation Center of Neuroregeneration, Nantong University, Nantong, China

8 Institute for Stem Cell and Regeneration, Chinese Academy of Sciences, Beijing, China

*Corresponding author. Tel: +86 0532 85950188; E-mail: hongjiang@qdu.edu.cn

**Corresponding author. Tel: +86 759 2387140; E-mail: jingjing.zhang@live.com

***Corresponding author. Tel: +86 10 64806335; E-mail: jwjiao@ioz.ac.cn

2007). FOXM1 is also a key cell cycle regulator, which promotes cell cycle progression and proliferation by up-regulating the transcription of cyclin D1 and cyclin B1 genes (Hu *et al*, 2014). FOXM1 has been previously shown to directly regulate genes with known roles in neocortical expansion, such as beta-catenin or ASPM (Zhang *et al*, 2011). FOXM1 isoforms, designated FOXM1A, FOXM1B, and FOXM1C, are formed by differential splicing of exon 6 (Va) and exon 9 (VIIa) (Laoukili *et al*, 2007). Human FOXM1 is alternatively spliced. Alternative splicing creates a new chimeric protein that provides an evolutionary advantage. We were concerned with the FOXM1A variant because human FOXM1 exon 9 is found in all apes and other primates but not in mice. However, the function of human FOXM1 in brain development remains unknown, and thus, we decided to explore its role by expressing this gene in mice.

Here, we have found that FOXM1 promotes the proliferation of neural progenitors, resulting in cortical expansion and folding in the mouse brain. We find that the human FOXM1-specific sequence plays a role in the generation of basal progenitor cells. Moreover, our data show that FOXM1 binds to the promoter of *Lin28a*, increasing the proliferative ability of neural progenitors. In addition, FOXM1 and LIN28A promote human neural precursor cell proliferation. Together, our study results reveal important functions of FOXM1 in the developing cerebral cortex, thus providing new insights into the molecular mechanisms of cortical expansion and folding by FOXM1 in the developing brain.

Results

The human gene FOXM1 is expressed in neural progenitors

To explore the function of FOXM1 in brain development, we first assessed the expression of FOXM1 in the fetal human brain (GW15-16). Immunofluorescence staining of GW15-16 cortical tissue sections showed that FOXM1 is expressed in VZ, iSVZ, and oSVZ (Fig 1A). In addition, FOXM1 was colocalized with NESTIN and SOX2 in human neural progenitor cells (Fig 1B and C), suggesting a role for FOXM1 in cortical development. To demonstrate that human FOXM1 (hFOXM1) is expressed in the mouse brain, human

FOXM1 plasmid was expressed in the lateral ventricle of mouse neocortex at embryonic day 13, using *in utero*. The results showed that hFOXM1 is expressed in the mouse brain (Appendix Fig S1A). To investigate the potential role of hFOXM1 in corticogenesis, human FOXM1 and mouse *Foxm1* plasmids were delivered to E13 brains using *in utero* electroporation. We found that the number of GFP⁺Pax6⁺/GFP⁺ neural precursor cells expanded within SVZ region in mice at E15 (Fig 1D–F). The increased proliferation capacity of neural progenitor cells leads to an expansion region above SVZ that resembled an enlarged SVZ. Sox2⁺ neural progenitors exhibited the typical morphology of basal RGCs, which had basal but not apical processes (Fig EV1A and B). Using *in utero* electroporation, the human FOXM1 plasmid was expressed in the lateral ventricle of the mouse neocortex at embryonic day 13. We observed deformation of the cortical surface at regions containing electroporated cells at three days postnatal (P3). Cux1 and Ctip2 immunofluorescent staining showed that electroporated GFP⁺ cell expressed upper layers (Figs 1G and EV1C). To further explore whether the changes in the cortex are caused by accelerated cell migration, we performed *in utero* electroporation experiment. The human FOXM1 plasmid and mouse *Foxm1* plasmid delivered to E13 and E15 brains, sacrificed the pups at P0 or P3. We found that the overexpressing of hFOXM1 has no an accelerated cell migration phenotype (Fig EV1D–F; Appendix Fig S1B). These results suggested that structure changes are not generated by neurons migrating into the area.

Human gene FOXM1 expression causes cortical expansion and folding in mice

To further investigate the function of FOXM1 in cortical development, we generated conditional knock-in mice that expressed the human FOXM1 gene using Nestin-Cre (Fig EV2A). Western blotting showed that the expression of FOXM1 was increased at P0 in the FOXM1 conditional knock-in mouse (*hFOXM1*^{f/+}-NesCre; *hFOXM1*-cKI) brains (Fig EV2B). Thus, *hFOXM1*-cKI mice were used for further analysis. We examined the brains of postnatal day 0 (P0) *hFOXM1*-cKI pups and found that in the whole brain comparison between *hFOXM1*-cKI mice and WT mice. There was a moderate enlargement in the size, cortical thickness, and in brain/body

Figure 1. FOXM1 is expressed in the human embryonic cerebral cortex and induces formation of gyrus-like structure.

- A The expression pattern of FOXM1 in fetal human cortex at GW15. VZ, ventricular zone; ISVZ, inner subventricular zone; OSVZ, outer subventricular zone. Right panels show higher magnification images. Arrows show that FOXM1⁺ cells were colocalized with SOX2⁺ cells. Scale bars, 100 μ m (left); 50 μ m (right).
- B Staining for NESTIN and FOXM1 in human neural progenitor cells cultured *in vitro*. Down panels show higher magnification images. Scale bars, 50 μ m (up); 10 μ m (down).
- C Staining for SOX2 and FOXM1 in human neural progenitor cells cultured *in vitro*. Down panels show higher magnification images. Dashed shapes show that FOXM1⁺ cells were colocalized with SOX2⁺ cells in human neural progenitor. Scale bars, 50 μ m (up); 10 μ m (down).
- D Staining for Pax6 in E15.5 mice after IUE at E13.5. Arrowheads indicate Pax6⁺ cell in enlarged SVZ. Right panels show higher magnification images. VZ, ventricular zone; SVZ, subventricular zone; IZ, intermediate zone; CP, cortical plate. Scale bars, 50 μ m (left); 20 μ m (right).
- E Graph shows the percentage of Pax6⁺ cells among GFP⁺ cells ($n = 5$ each group; two-tailed unpaired *t*-test, control vs. hFOXM1, $P = 0.0032$; mFoxm1 vs. hFOXM1, $P = 0.0121$).
- F Graph shows the percentage of Pax6⁺ cells among GFP⁺ cells in enlarged SVZ ($n = 5$ each group; two-tailed unpaired *t*-test, control vs. hFOXM1, $P < 0.0001$; mFoxm1 vs. hFOXM1, $P < 0.0001$).
- G Staining for upper neuron marker Cux1 in P3 mice after IUE at E13.5. Arrowhead and asterisk indicate deformation of the cortical surface at regions containing electroporated cells. Right panels show higher magnification images. Arrows show GFP⁺ Cux1⁺ double-positive cells. Scale bars, 100 μ m (left); 20 μ m (right).

Data information: At least three biological replicates are shown. Data are represented as means \pm SEM. Two-tailed unpaired Student's *t*-test, * $P < 0.05$. ** $P < 0.01$. *** $P < 0.001$.

Source data are available online for this figure.

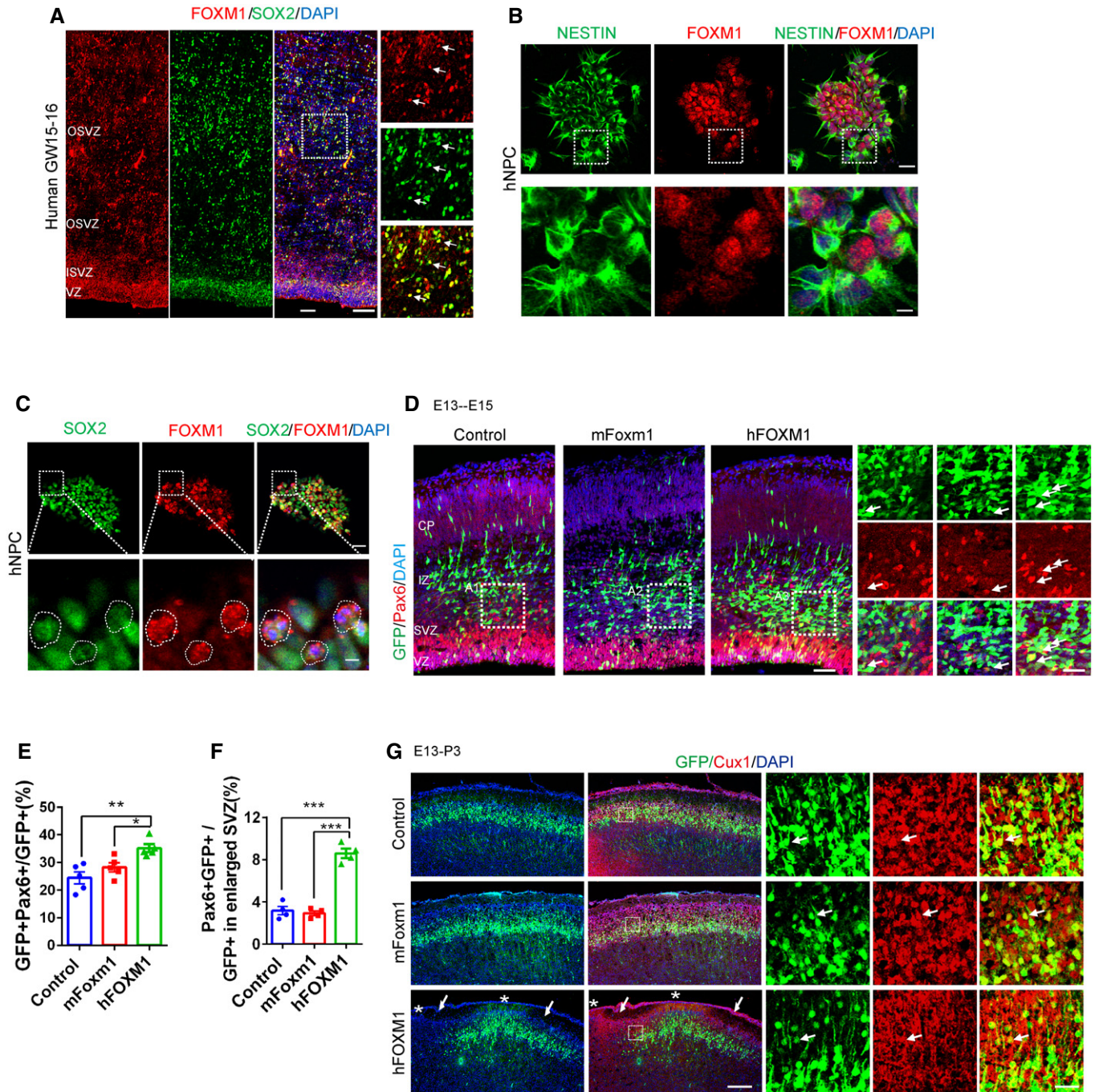


Figure 1.

weight at P0 (Fig 2A–D). We observed that forty percent of hFOXM1-cKI mice exhibited gyrus-like phenotypes in various degrees (Fig 2E). The gyrification index (GI) is a measure of the degree of folding. The gyrification index (GI) is a ratio of the lengths of the total to that of the superficially exposed cortical surface (Pillay & Manger, 2007; Zilles et al, 2013). The quantification of the GI was analyzed in pre-selected hFOXM1-cKI mice with folding. Our data revealed that local GI increased to 1.12 in hFOXM1-cKI mice compared with WT mice (Fig 2F). In addition, we observed an increase in Satb2⁺ upper layer neurons and Ctip2⁺ deeper neurons in

hFOXM1-cKI mice (Fig 2G–I). Immunostaining for NeuN (pan-neuronal marker) and S100β (astrocyte marker) and Western blotting for Tuj1, NeuN, Aldh1l11, Gfap, and Mbp showed that there was a significant increase in the neuronal cell number but no significant difference in the number of astrocytes and oligodendrocytes between hFOXM1-cKI and WT mice (Fig EV2C–G), indicating that cortex expansion and folding are caused by neurons and not astrocytes and oligodendrocytes. We observed the structure of gyrus-like brain slices in P3 knock-in mice and found that Cux1⁺ upper layer neurons were increased in P3 hFOXM1-cKI mice (Fig 2J–L). To

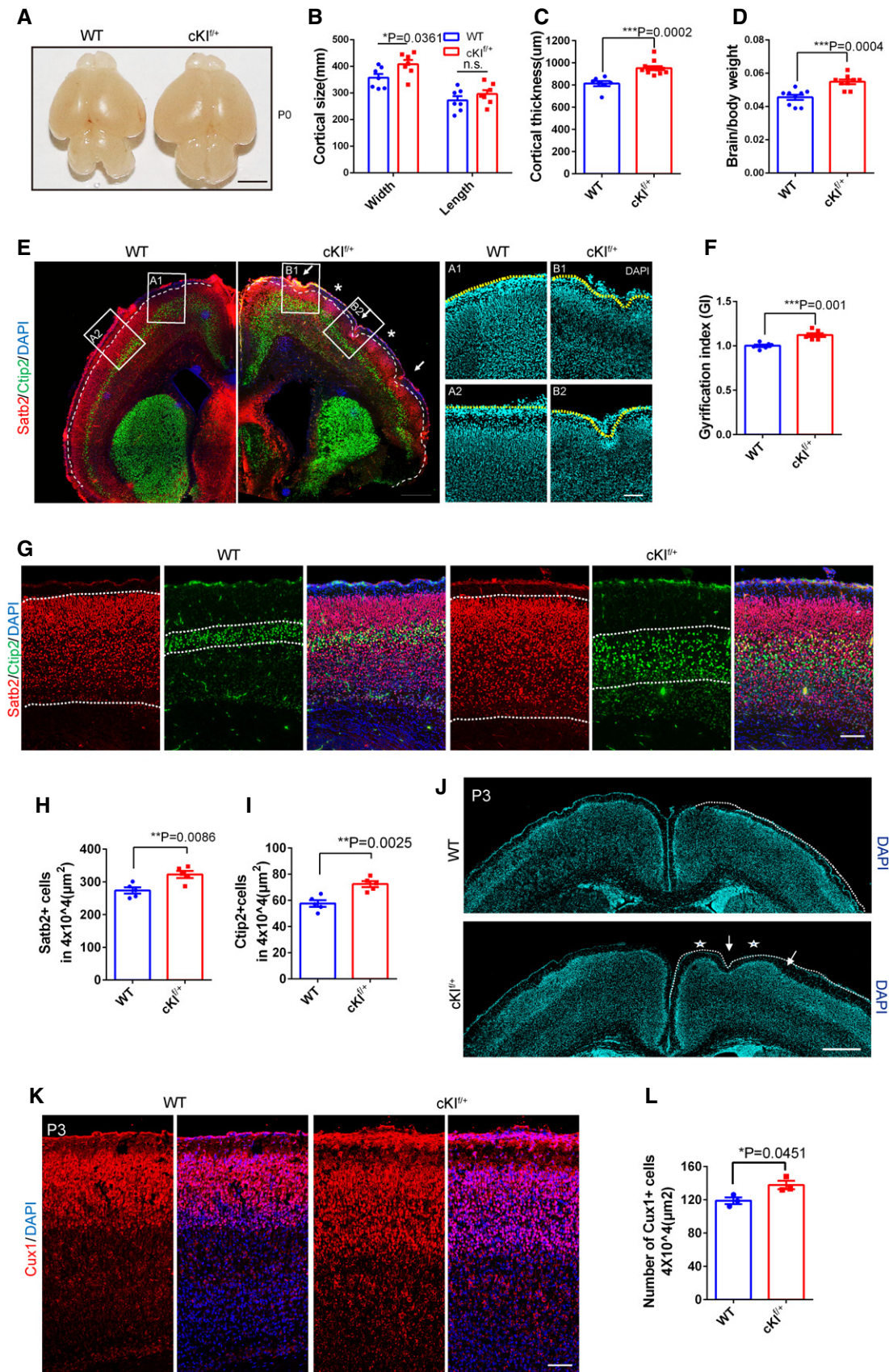


Figure 2.

Figure 2. Cortical expansion and folding are induced by human *FOXM1* expression in mice.

- A Representative images of whole brains from wild-type (WT) and *hFOXM1^{f/+}-NesCre* (*hFOXM1*-cKI) mice pups at P0. Scale bar, 100 μ m.
- B Quantification of cortical width and length at P0 (WT $n = 7$; *hFOXM1*-cKI $n = 7$; two-tailed unpaired t -test, $P = 0.0361$ for width, $P = 0.2866$ for length).
- C Quantification of brain/body weight at P0 (WT $n = 9$; *hFOXM1*-cKI $n = 9$; two-tailed unpaired t -test, $P = 0.0004$).
- D Quantification of cortex thickness at P0 (WT $n = 7$; *hFOXM1*-cKI $n = 11$; two-tailed unpaired t -test, $P = 0.0002$).
- E Staining for *Satb2* and *Ctip2* in P0 WT and *hFOXM1*-cKI mice folding structure. Asterisks indicate gyrus, and arrows indicate sulcus structures. A1, A2, B1, and B2 (DAPI) are high-magnification images. Scale bars, 200 μ m(left); 100 μ m(right).
- F Quantification of GI of WT and *hFOXM1*-cKI mice pups at P0. The quantification of the GI was analyzed in pre-selected *hFOXM1*-cKI mice with folding. ($n = 6$ each group; two-tailed unpaired t -test, $P = 0.0010$).
- G Staining for *Satb2* and *Ctip2* in P0 WT and *hFOXM1*-cKI mice. White dash lines represent the positive area. Scale bar, 100 μ m.
- H Graph shows the number of *Satb2*⁺ cells in $4 \times 10^4 \mu\text{m}^2$ at P0 (WT $n = 5$; *hFOXM1*-cKI $n = 5$; two-tailed unpaired t -test, $P = 0.0086$).
- I Graph shows the number of *Ctip2*⁺ cells in $4 \times 10^4 \mu\text{m}^2$ at P0 (WT $n = 5$; *hFOXM1*-cKI $n = 5$; two-tailed unpaired t -test, $P = 0.0025$).
- J Staining for DAPI in P3 WT and *hFOXM1*-cKI mice. Asterisks indicate gyrus, and arrows indicate sulcus structures. Scale bars, 500 μ m.
- K Staining for *Cux1* in P0 WT and *hFOXM1*-cKI mice. Scale bar, 100 μ m.
- L Graph shows the number of *Cux1*⁺ cells in $4 \times 10^4 \mu\text{m}^2$ at P0 (WT $n = 3$; *hFOXM1*-cKI $n = 3$; two-tailed unpaired t -test, $P = 0.0451$).
- Data information: At least three biological replicates are shown. Data are represented as means \pm SEM. Unpaired two-tailed Student's t -test. * $P < 0.05$. ** $P < 0.01$. *** $P < 0.001$.

analyze apoptosis occurring early postnatally in mice (Wong & Marin, 2019), we performed terminal-deoxynucleotidyl transferase dUTP end-labeling (TUNEL) assays at P3 and Western blot experiments at P5. We found that there was a slight increase in *hFOXM1* knock-in mouse TUNEL⁺ cells compared with wild type, but the increase was not statistically significant. Western blotting showed that there was no difference in caspase 3 and cleaved caspase 3. Therefore, there appears to be no effect in *hFOXM1* knock-in mice on apoptosis in the second wave of cell death that naturally occurs early postnatally in mice (Appendix Fig S2A–D). Together, these results suggest that *hFOXM1* promotes the formation of cortical folding formation.

Human *FOXM1* expression promotes the generation of cortical basal progenitor cells in mice

To determine the causes of cortical folding induced by the human *FOXM1* gene, we chose the neurogenic peak as the study site. We observed a marked increase in the population of Pax6⁺ neural progenitors in the enlarged SVZ of E15 *hFOXM1*-cKI mice. Pax6⁺ p-Vim⁺ neural progenitors exhibited the typical morphology of basal RGCs, which had basal but not apical processes (Fig 3A–C). In

addition, Sox2⁺ progenitors were also increased in the enlarged SVZ of E15 mice (Fig 3D and E), which was consistent with transient expression. Tbr2⁺ progenitors were also increased in the enlarged SVZ of E15 mice (Fig 3F and G). HOPX is a basal radial glial marker (Pollen *et al*, 2015; Ostrem *et al*, 2017). We observed that HOPX⁺ cells were increased and extended into the enlarged SVZ compared with WT mice (Fig 3H and I). Then, we measured the protein level in the E15 *hFOXM1*-cKI mouse neocortex and observed that the expression levels of Sox2 and Pax6 and HOPX were increased (Fig EV3A and B). These results suggest that human *FOXM1* expression in mice increases basal progenitor cells during cortical development.

It was previously reported that the number of progenitor cells is related to the cell cycle (Matthias Groszer *et al*, 2006). Therefore, we assessed the cell proliferation activity of neural progenitor cells in the developing cortex. BrdU pulsing showed an increase in the number of BrdU⁺ basal progenitors in *hFOXM1*-cKI mice at E15 (Fig EV3C and D). Ki67⁺ proliferating cells were also increased in *hFOXM1*-cKI mice (Fig 3J and K). Mitotic cell (pH3⁺) immunofluorescence showed that quantified apical mitoses had a slight increase in *hFOXM1*-cKI mice, but no statistically significant. Quantified basal mitoses were increased in *hFOXM1*-cKI mice (Fig EV3E and

Figure 3. Cortical basal progenitor cells are increased in *FOXM1* conditional knock-in mice.

- A Staining for Pax6 and p-Vim in E15 WT and *hFOXM1*-cKI mice. The right A and B are high-magnification images. Arrows indicate double positive of Pax6⁺ p-Vim⁺ cells with cells with a basal process (arrowheads). Scale bars, 50 μ m (left); 5 μ m (right).
- B Graph shows the percentage of Pax6⁺ cells in enlarged SVZ ($n = 6$ each group; two-tailed unpaired t -test, $P = 0.0002$).
- C Graph shows the number of Pax6⁺ p-Vim⁺ cells in $4 \times 10^4 \mu\text{m}^2$ in enlarged SVZ ($n = 6$ each group; two-tailed unpaired t -test, $P = 0.0003$).
- D Staining for Sox2 in E15 WT and *hFOXM1*-cKI mice. Scale bar, 50 μ m.
- E Graph shows the number of Sox2⁺ cells in $4 \times 10^4 \mu\text{m}^2$ in enlarged SVZ (WT $n = 3$; *hFOXM1*-cKI $n = 4$; two-tailed unpaired t -test, $P = 0.0292$).
- F Staining for Tbr2 in E15 WT and *hFOXM1*-cKI mice. Scale bar, 50 μ m.
- G Graph shows the number of Tbr2⁺ cells in $4 \times 10^4 \mu\text{m}^2$ in enlarged SVZ (WT $n = 6$; *hFOXM1*-cKI $n = 9$; two-tailed unpaired t -test, $P = 0.0003$).
- H Staining for HOPX in E15 WT and *hFOXM1*-cKI mice. Scale bar, 50 μ m.
- I Graph shows the number of HOPX⁺ cells in $4 \times 10^4 \mu\text{m}^2$ in enlarged SVZ ($n = 4$ each group; two-tailed unpaired t -test, $P = 0.0044$).
- J Staining for Ki67 in E15 WT and *hFOXM1*-cKI mice. Scale bar, 50 μ m.
- K Graph shows the percentage of Ki67⁺ cells in enlarged SVZ ($n = 4$ biological replicates; two-tailed unpaired t -test, $P = 0.0038$).
- L The experimental scheme and staining for BrdU and EdU in E15 WT and *hFOXM1*-cKI mice. White arrows represent BrdU and EdU double-positive cells. Scale bars, 50 μ m(left); 20 μ m(right).
- M Graph shows the percentage of BrdU and EdU double-positive cells in E15 WT and *hFOXM1*-cKI mice ($n = 6$ each group; two-tailed unpaired t -test, $P = 0.0413$).
- Data information: At least three biological replicates are shown. Data are represented as means \pm SEM. Unpaired two-tailed Student's t -test. * $P < 0.05$. *** $P < 0.001$.

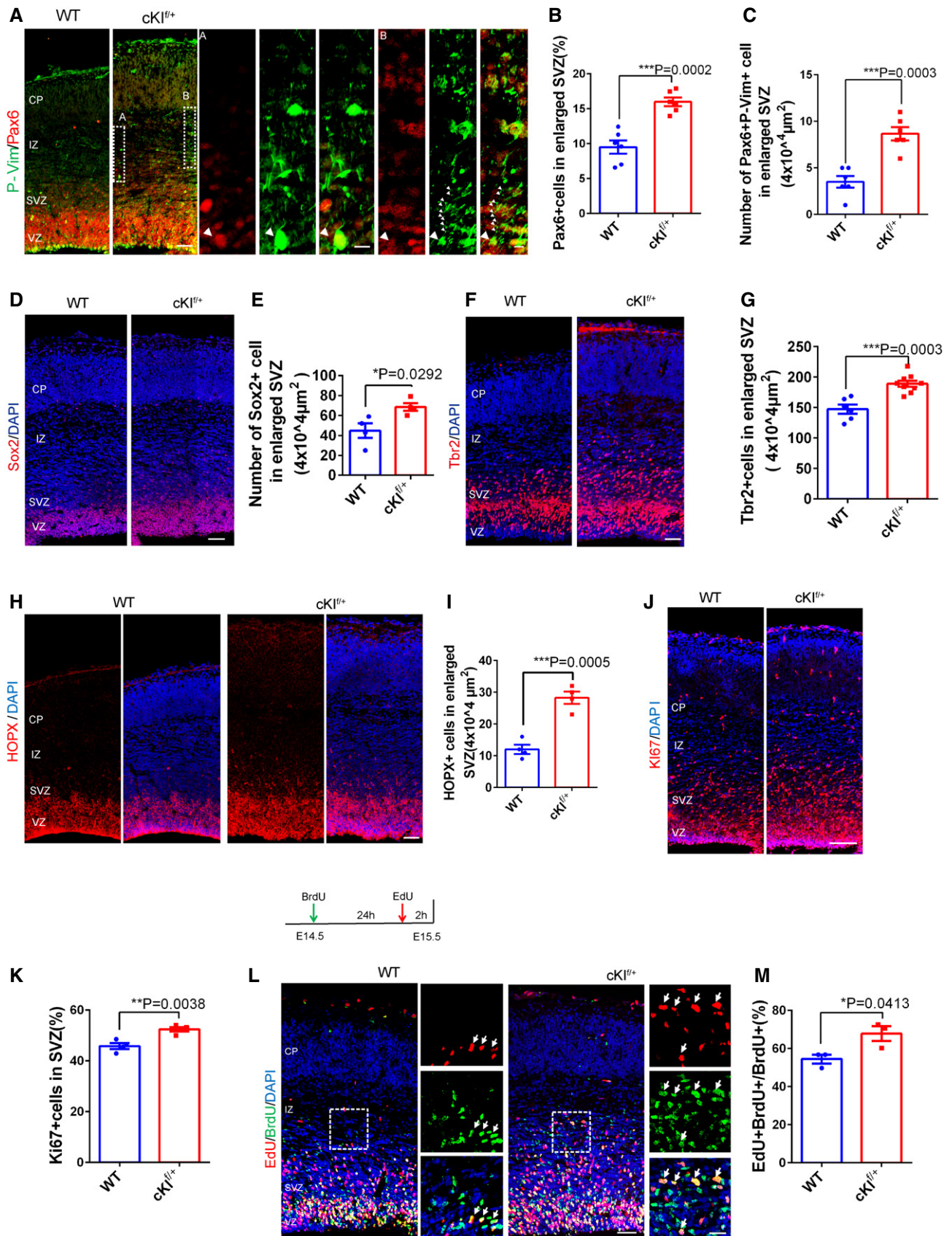


Figure 3.

F). These results suggest that human FOXM1 increases neural precursor cell proliferative potential. We next examined cell cycle re-entry by a BrdU/EdU double pulsing analysis. These results showed an EdU⁺ BrdU⁺ basal progenitor increase in hFOXM1-cKI mice (Fig 3L and M). Together, these results suggest that FOXM1 promotes basal RGC production.

The human FOXM1-specific sequence plays a key role in the generation of basal progenitor cells

To further explore the cause of the formation of cortical basal progenitor cells, we compared the homology of the human FOXM1 gene and the mouse Foxm1 gene. By comparing the expression of FOXM1 in mice and humans in different regions (Fietz et al, 2012), we found that the expression of FOXM1 at mVZ and hVZ regions has a comparable level ($P = 0.3880$), but there are significant differences at mSVZ and hiSVZ regions and mSVZ and hoSVZ regions (Appendix Tables S1 and S2). Compared to mouse Foxm1, human FOXM1 essentially appears to have an additional 114 nt encoding 38 aa that comprises exon 9. We wondered whether this unique sequence plays an important role in the proliferation of basal progenitor cells. Therefore, we constructed a human gene FOXM1 mutant (hFOXM1^{Δexon9}) and a mouse gene Foxm1 mutant (mFoxm1^{+hexon9}) (Fig 4A). We used a lentivirus to infect mouse primary neural precursor cells to measure the potential effect of human FOXM1 exon 9 on basal progenitor cell proliferation. Immunofluorescence staining and Western blot analysis were performed after three days of culture in proliferation medium. We found that overexpression of hFOXM1 increased the percent of HOPX⁺ cells in mouse primary neural progenitor cells, but expressing a mutated form of hFOXM1 with the deletion of amino acids 423–441 (hFOXM1^{Δexon9}) caused a loss of this function (Fig 4B and C). In addition, expressing a mutated form of mFoxm1 with the insertion of human amino acids 423–441 (mFoxm1^{+hexon9}) increased the percent of HOPX⁺ cells, while the overexpression of mFoxm1 did not

lead to a significant change compared with the control (Fig 4D and 4E). Western blotting showed that the expression levels of HOPX were obviously increased in human FOXM1 lentivirus-infected mouse primary neural progenitor cells, while the expression levels of HOPX were not significantly increased compared with the control in human FOXM1^{Δexon9} lentivirus-infected mouse primary neural progenitor cells (Fig 4F and G). Moreover, Western blotting showed that the expression of HOPX was obviously increased in the mouse primary neural progenitor cells infected with the FOXM1 mutant with the insertion of exon 9 (Fig 4H and I). Next, we performed *in utero* electroporation with hFOXM1, mouse Foxm1 and hFOXM1^{Δexon9} at embryonic day 13. Only hFOXM1 has an increase in Tbr2⁺ precursor cells above SVZ region in mice at E15, suggesting that human exon 9 is beneficial to the formation of basal progenitor cells (Fig 4J and K). These results suggest that the unique human FOXM1 sequence is beneficial to the generation of progenitor cells.

Human FOXM1 regulates neurogenesis by targeting Lin28a

Because the increased proliferation ability of NPCs is necessary for cortical expansion and folding formation in hFOXM1-cKI mice, we further explored the mechanism by which hFOXM1 regulates the proliferation of NPCs and the role of this additional exon 9 in the increased neurogenic phenotype. First, we examined whether hFOXM1 exon 9 promotes precursor cell proliferation driven by protein stability. We performed a cycloheximide (CHX) pulse-chase experiment with 293FT and found that hFOXM1^{Δexon9} was not significantly different from hFOXM1 (Appendix Fig S3A and B). In addition, mFoxm1 was not significantly different from hFOXM1 (Appendix Fig S3C and D). These results showed that the role of exon 9 was not driven by increasing protein stability. Then, we examined changes in transcription levels. Bulk RNA sequencing was used to analyze the genome-wide changes resulting from the cerebral cortices of E15 hFOXM1-cKI mice and wild-type littermates.

Figure 4. Human FOXM1 unique sequence promotes the generation of basal progenitor cells.

- A Structure of human FOXM1 gene, mouse Foxm1 gene, mutant of human gene FOXM1 (hFOXM1^{Δexon9}), and mutant mouse gene Foxm1 (mFoxm1^{+hexon9}).
- B Cell immunostaining for HOPX in control, hFOXM1-FL, and mutants in mice primary neural progenitors 3 days following lentiviral infection. White arrows represent GFP HOPX double-positive cells. Scale bar, 50 μm.
- C Graph shows the percentage of HOPX⁺ cells among GFP⁺ cells (control $n = 3$; hFOXM1-FL $n = 6$; hFL^{Δexon9} $n = 5$; one-way ANOVA, $F(2, 12) = 29.13$, control vs. hFOXM1, $P = 0.0002$; control vs. hFOXM1^{Δexon9}, $P = 0.9080$).
- D Cell immunostaining for HOPX in control, mFoxm1-FL, and mutants in mice primary neural progenitors 3 days following lentiviral infection. White arrows represent GFP HOPX double-positive cells. Scale bar, 50 μm.
- E Graph shows the percentage of HOPX⁺ cells among GFP⁺ cells (control $n = 4$; mFoxm1-FL $n = 6$; mFL^{+hexon9} $n = 4$; one-way ANOVA, $F(2, 11) = 8.163$, control vs. mFoxm1, $P = 0.4747$, control vs. mFoxm1^{+hexon9}, $P = 0.0066$).
- F Western blot analysis for basal RG marker (HOPX) in control, hFOXM1 and mutants in mice primary neural progenitors 3 days after lentiviral infection. β-actin was detected as loading control.
- G Statistics of relative intensity of HOPX ($n = 3$ biological replicates, one-way ANOVA, $F(2, 6) = 5.084$, control vs. hFOXM1 $P = 0.0435$, control vs. hFOXM1^{Δexon9} $P = 0.3991$ for HOPX).
- H Western blot analysis for HOPX in control, mFoxm1, and mutants in mice primary neural progenitors 3 days after lentiviral infection. β-actin was detected as loading control.
- I Statistics of relative intensity of HOPX ($n = 3$ biological replicates; one-way ANOVA $F(2, 6) = 8.111$, control vs. mFoxm1, $P = 0.6024$, control vs. mFoxm1+hexon9, $P = 0.0192$ for HOPX).
- J Staining for Tbr2 in E15.5 mice after IUE at E13.5. Down panels show higher magnification images. White arrows represent GFP and TBR2 double-positive cells. Scale bars, 50 μm.
- K Graph shows the percentage of GFP⁺Tbr2⁺/GFP⁺ in enlarged SVZ ($n = 3$ each group; one-way ANOVA, $F(3, 8) = 8.787$, $P = 0.0065$).

Data information: At least three biological replicates are shown. Data are represented as means ± SEM. One-way ANOVA was used for statistical analysis. n.s., no significant, * $P < 0.05$. ** $P < 0.01$. *** $P < 0.001$.

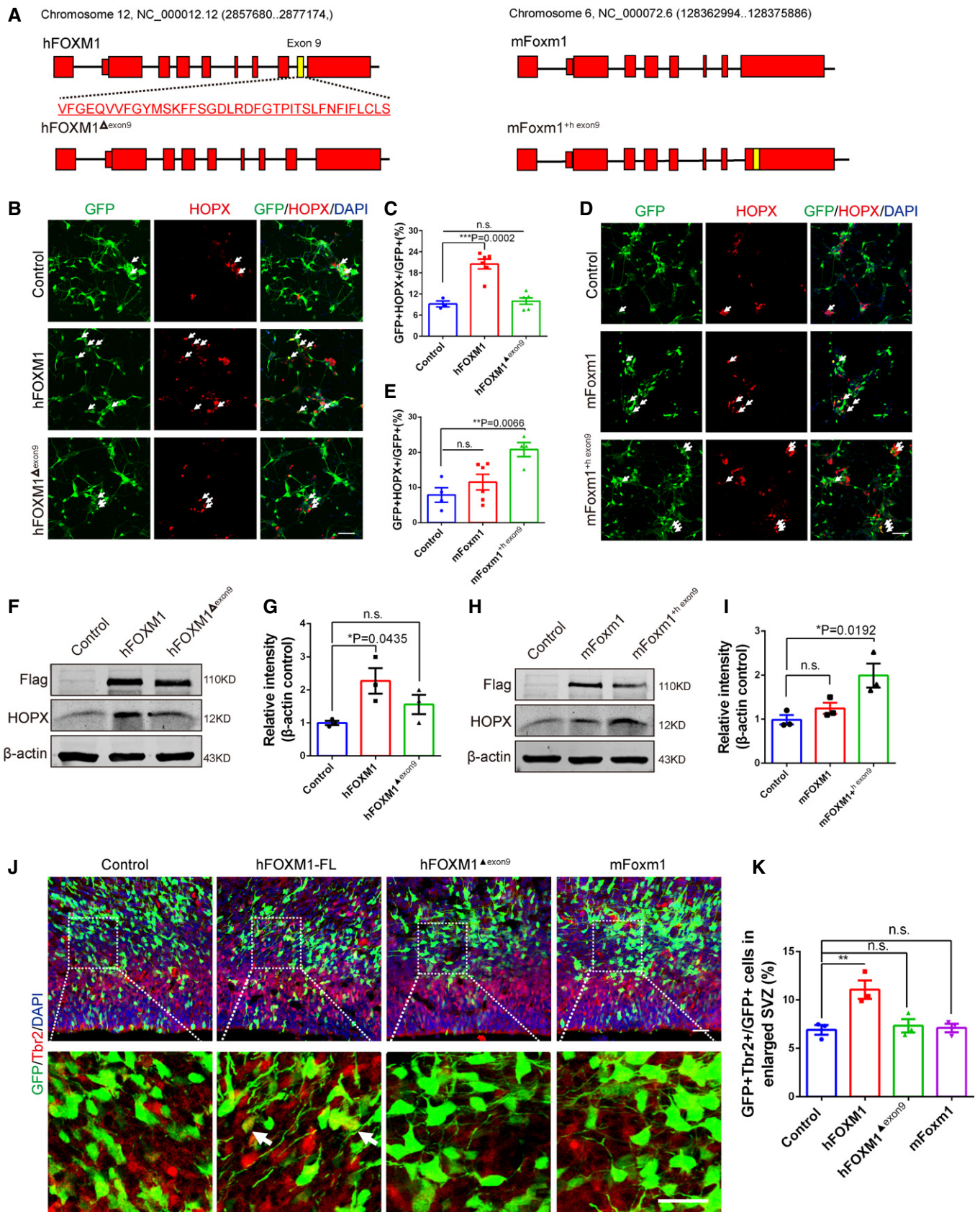


Figure 4.

Gene ontology analysis of the up-regulated genes showed obvious enrichment of biological processes related to development and proliferation, such as regulation of the cell cycle process and the development process and cell proliferation (Fig 5A). The down-regulated genes exhibited enrichment of biological processes related to the negative regulation of cell proliferation and developmental processes (Fig 5B). Cell proliferation reflects a consequence of a complex interaction among these positive and negative regulator factors (Johnson, 1994). Negative regulators of cell proliferation were down-regulated, providing support that FOXM1 promotes cell proliferation during cortical development. Volcano plots revealed differences in the gene transcripts between the hFOXM1 conditional knock-in mice and wild-type mice (Fig 5C). One of these genes was the *Lin28a* gene, a well-known RNA-binding protein. Previous studies have shown that Lin28a affects developmental events during neurulation in mice (Miyazawa et al, 2019) and contributes to the regeneration of exhausted Sox2 progenitors in mammals. Therefore, it may perform a certain function in neurodevelopment. Lin28a was selected as the candidate downstream molecule. Western blot and immunofluorescent staining showed that the expression of Lin28a was obviously increased in hFOXM1-cKI mice (Fig 5D and Appendix Fig S4A). Next, we examined whether FOXM1 binds to *Lin28a* using chromatin immunoprecipitation (ChIP) experiments. We designed 6 pairs of primers targeting different regions of the *Lin28a* gene (from -5 kb to the coding sequence) for enrichment analysis (Fig 5E). The results indicated that human FOXM1 was significantly enriched in a region of the *Lin28a* promoter surrounding position -2K from the transcriptional start site (TSS). hFOXM1 was also significantly enriched in a region of the hLIN28A promoter surrounding position -2K from the transcriptional start site (TSS) (Appendix Fig S4B), but mFoxm1 and the deletion of exon 9 reduced the binding to *Lin28a* (Fig 5E), suggesting that exon 9 enhances the affinity for DNA binding sites.

We further investigated the role of LIN28A in cortical development and found that the hLIN28A protein was broadly expressed in SOX2⁺ progenitors (Appendix Fig S5A and B). The human LIN28A plasmid was expressed in the lateral ventricle of the mouse neocortex at embryonic day 13 using in utero electroporation. We observed that Sox2⁺ cells increased in the enlarged SVZ region at E15 compared with the control group (Fig 5F–H). We then constructed LIN28A short hairpin RNA (LIN28A-shRNA) to suppress its expression (Fig EV4A and B). Compared to the control, knock-down of LIN28A disrupted the increase in BrdU⁺ cell number induced by the

transient expression of FOXM1 (Fig EV4C and D). LIN28A-shRNA reduced the number of Sox2⁺ neural precursor cells in hFOXM1-cKI mice (Fig 5I and J). Together, these results suggested that LIN28A is an important downstream target gene of FOXM1.

FOXM1 and LIN28A regulate human neural precursor cell proliferation

To determine the role of FOXM1 in human neural precursor cells (NPCs), we generated FOXM1 knockout human ESC lines based on CRISPR/Cas9 gene editing (Fig EV5A and B) and then differentiated them into human neural precursor cells (Fig 6A). Human neural precursor cells were digested into single cells and maintained in culture 3 days before immunofluorescence staining. We observed that hNPC-FOXM1^{-/-} had a smaller clone size compared with hNPC-FOXM1^{+/+} (Fig 6B and C). We found that human neural precursor cells were increased by hFOXM1 lentiviral infection (Fig EV5C and D). To detect the role of LIN28A in human cortical development, we performed BrdU tracking experiment. Immunofluorescence staining showed that knock-down of LIN28A reduced the number of BrdU⁺ HOPX⁺ and BrdU⁺ TBR2⁺ human neural precursor cells (Appendix Fig S6A–D). These results suggest that knock-down of LIN28A inhibits the proliferation of human neural progenitor cells. Rescue experiments were performed in FOXM1 knockout cell line. Human ESCs were differentiated into human NPCs, followed by control empty vector, FOXM1 or LIN28A lentivirus infection. Western blotting was performed 3 days after lentiviral infection. We observed that the expression levels of SOX2, PAX6, and HOPX were increased in FOXM1- or hLIN28A-infected human NPC-FOXM1^{-/-} cells (Fig 6D and E). These results suggest that overexpression of FOXM1 or LIN28A can rescue the reduction in the proliferation of FOXM1 knockout human NPC lines. To further verify the reason for the increase of human NPC, we added BrdU for 2h before analysis. Similar results were obtained by co-immunostaining with anti-BrdU and anti-HOPX antibodies (Fig EV5E and F). Thus, we conclude that FOXM1 and LIN28A play roles in human neural precursor cell proliferation.

Discussion

In this study, we find that expression of human gene FOXM1 in mice increased neural progenitor cell expansion, caused cortical

Figure 5. FOXM1 regulates proliferation of neural precursor cells through *Lin28a*.

- A Gene ontology analysis for up-regulated genes based on RNA-seq data in E15 hFOXM1-cKI mice.
- B Gene ontology analysis for down-regulated genes based on RNA-seq data in E15 hFOXM1-cKI mice.
- C Volcano plots show the gene expression states. The yellow dots are the up-regulated genes, and the blue dots are the down-regulated genes. The *Lin28a* gene (red dot) is significantly up-regulated.
- D Western blot analysis for Lin28a in cortex of E15 WT and hFOXM1-cKI mice. β -actin was detected as loading control.
- E CHIP analysis for hFOXM1, mFoxm1, and hFOXM1^{Δexon9} binding to the region of the *Lin28a* promoter in the N2A cells. ($n = 3$ biological repeats).
- F Staining for Sox2 in E15.5 mice after IUE at E13.5. Arrowheads indicate Sox2⁺ cell in enlarged SVZ. Scale bar, 50 μ m.
- G Graph shows the percentage of Sox2⁺ cells among GFP⁺ cells in enlarged SVZ ($n = 3$ each group; two-tailed unpaired t -test, $P = 0.0154$).
- H Graph shows the percentage of Sox2⁺ cells among GFP⁺ cells ($n = 3$ each group; two-tailed unpaired t -test, $P = 0.0018$).
- I LIN28A-shRNA1 rescues the neuronal progenitor cell increase in hFOXM1-cKI mice. Brain slice staining for Sox2 two days after IUE at E13. Scale bar, 50 μ m.
- J Graph shows the percentage of Sox2⁺ cells among GFP⁺ cells ($n = 3$ each group; one-way ANOVA, $F(2, 6) = 11.32$, control-GFP(WT) vs. control-GFP (cKI^{f/f}), $P = 0.0105$; control-GFP (WT) vs. LIN28Ash1-GFP (cKI^{f/f}), $P = 0.7712$).

Data information: At least three biological replicates are shown. Data are represented as means \pm SEM. Student's t -test: * $P < 0.05$, ** $P < 0.01$.

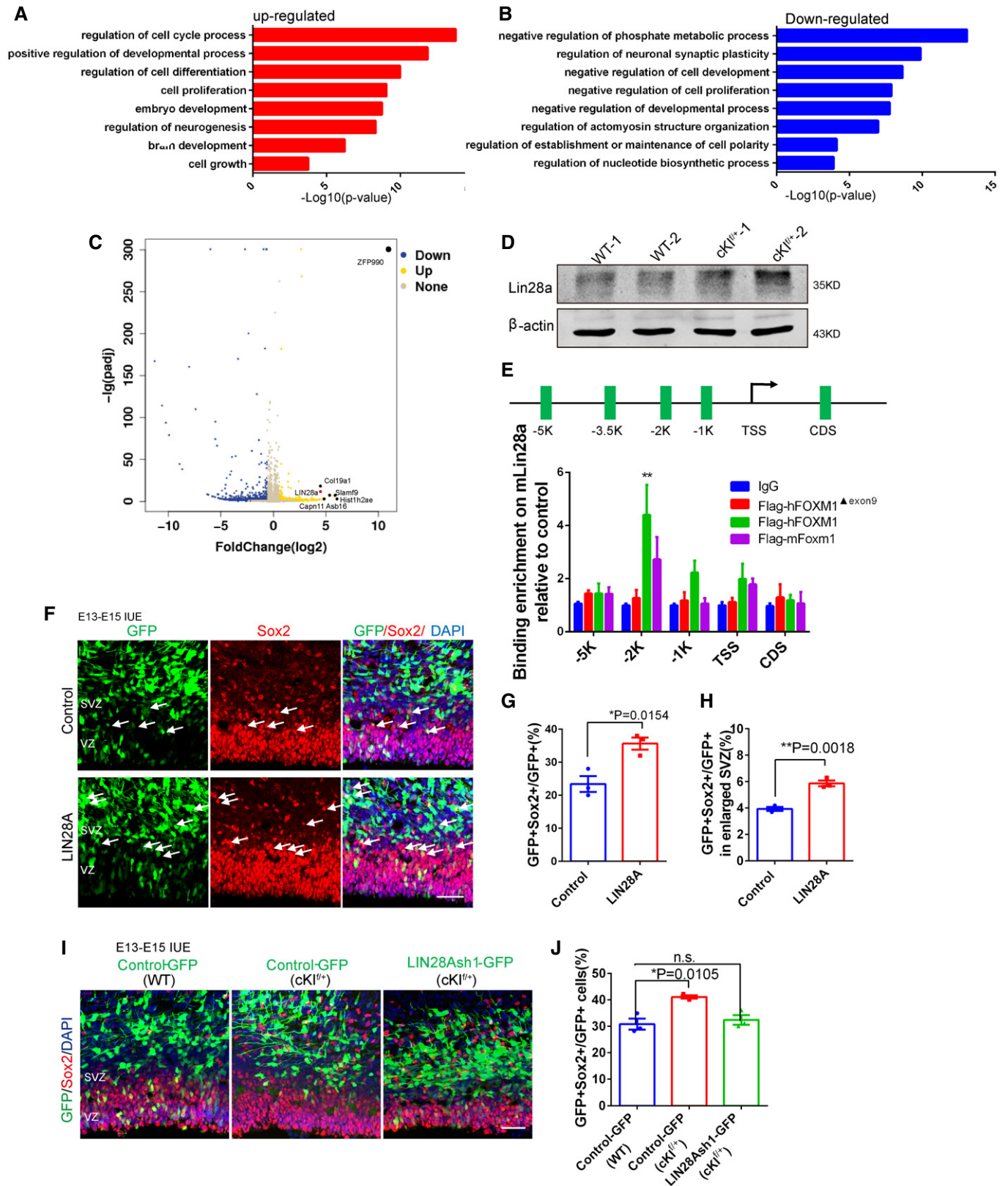


Figure 5.

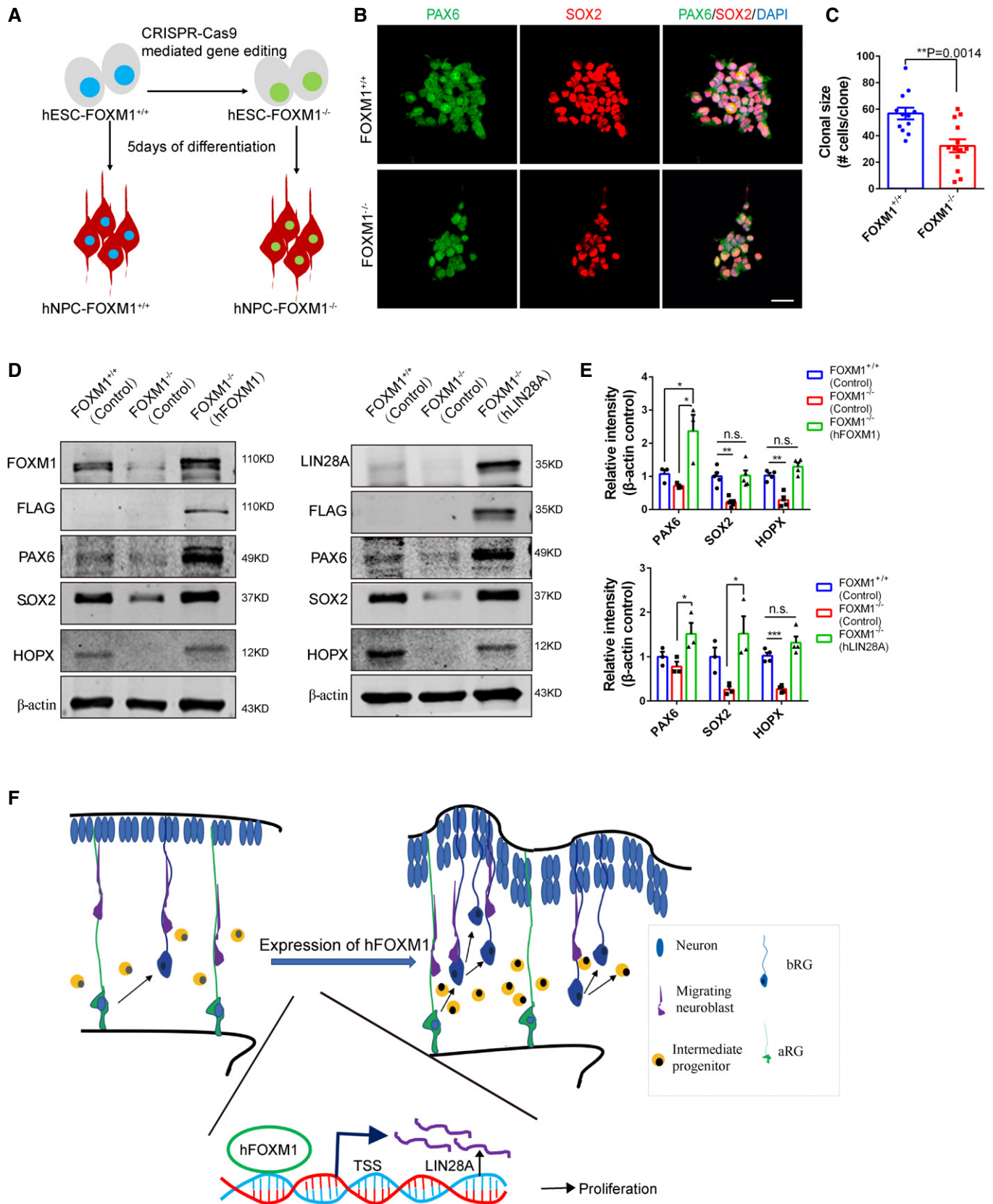


Figure 6.

Figure 6. LIN28A is downstream target of hFOXM1 and rescues the phenotype hFOXM1 knockout in human progenitor cell.

- A Schematic showing the method used to generate *FOXM1*^{+/+} and *FOXM1*^{-/-} human NPCs.
- B Representative cases of *FOXM1*^{+/+} and *FOXM1*^{-/-} NPCs clones. Scale bar, 20 μm.
- C Graph shows the number of cells per clone in *FOXM1*^{+/+} and *FOXM1*^{-/-} human NPCs (*FOXM1*^{+/+} *n* = 12; *FOXM1*^{-/-} *n* = 13; at least three biological replicates. two-tailed unpaired t-test, *P* = 0.0014).
- D Overexpression of *FOXM1* or *LIN28A* rescues the human neural progenitor cell reduction in *FOXM1*^{-/-} cell lines. Western blot analysis for SOX2, PAX6, and HOPX. β-actin was detected as loading control.
- E Statistics of relative intensity of SOX2, PAX6, and HOPX (PAX6: *n* = 3 biological replicates; one-way ANOVA, *F* (2,6) = 8.716, *FOXM1*^{-/-} (control) vs. *FOXM1*^{-/-} (hFOXM1), *P* = 0.0173, *FOXM1*^{+/+} (control) vs. *FOXM1*^{-/-} (hFOXM1), *P* = 0.0476. SOX2: *n* = 5 biological replicates; one-way ANOVA, *F* (2, 12) = 14.72, *FOXM1*^{+/+} (control) vs. *FOXM1*^{-/-} (control), *P* = 0.0015, *FOXM1*^{+/+} (control) vs. *FOXM1*^{-/-} (hFOXM1), *P* = 0.9906. HOPX: *n* = 4 biological replicates, one-way ANOVA *F* (2, 9) = 25.28, *FOXM1*^{+/+} (control) vs. *FOXM1*^{-/-} (control), *P* = 0.0018, *FOXM1*^{+/+} (control) vs. *FOXM1*^{-/-} (hFOXM1), *P* = 0.2211).
- F The model for the role of hFOXM1 in cerebral cortex. Human *FOXM1* expression causes neural precursor cells increase through up-regulating the level of LIN28A. The increased neural precursor cells subsequently increase in the number of newborn neurons and induce cortical extension and folding in mice.
- Data information: At least three biological replicates are shown. Data are represented as means ± SEM, unpaired Student's t-test, one-way ANOVA. n.s., no significant, **P* < 0.05, ***P* < 0.01, ****P* < 0.001.

thickening and cortical folding generation. We uncover an important mechanism of *FOXM1* by targeting *Lin28a* promoter, and thereby promoting the proliferation of neural precursor cells (Fig 6F).

Cortical expansion and folding reflect an increase in various subtypes of neural precursor cells and the proliferative capacity of neural progenitors including the apical RGC, the intermediate progenitors (IP), and basal RGC (Lui *et al*, 2011; Sun & Hevner, 2014; Dehay *et al*, 2015). Overexpression of β-catenin in neural progenitor cells can regulate cerebral cortical size (Chenn & Walsh, 2002). An expanded SVZ region (OSVZ) in gyrencephalic animals contains a new type of RG cell (bRGC), which has a greater capacity for proliferation (Fietz *et al*, 2010; Hansen *et al*, 2010; Dehay, 2014). Overproliferation of basal radial glial cells (bRGCs) increases cortical surface area and folding in primates (Reillo *et al*, 2011; Nonaka-Kinoshita *et al*, 2013). Recently, some studies have shown that human-specific genes promote cortical progenitor proliferation and expansion through different mechanisms by inhibiting histone methylation activity or glutaminolysis regulation (Deyama & Duman, 2020; Hou *et al*, 2021). Increased proliferation capacity of cortical progenitors is critical for cortical expansion. In our study, human *FOXM1* increased the number of neural precursor cells, especially *Tbr2*⁺ and *HOPX*⁺ cells by shortening cell cycle. These findings suggest that cortical thickening in human *FOXM1*-cKI mice is the accumulation of proliferation of multiple precursor cells. Human *FOXM1* increased the number of upper layer and deeper layer neurons, which caused cortical expansion and folding. The human *FOXM1*-specific sequence increased the number of basal progenitor cells and increased the number of S-phase progenitor cells. These results may explain why human *FOXM1* inserted into mice can induce folding, which was not observed in normal mouse *Foxm1* expression. We found an important mechanism by which *FOXM1* targeted *Lin28a* promoter, increased *Lin28a* mRNA expression, and ultimately promoted the proliferation of neural precursor cells. *LIN28A* protein is critical for stem cell self-renewal, organismal growth, somatic cell reprogramming, and regeneration (Shyh-Chang & Daley, 2013; Herrlinger *et al*, 2019). *Lin28a*-shRNA reduced the number of neural precursor cells in hFOXM1 conditional knock-in mice, and overexpression of *Lin28A* rescued the proliferation reduction of *Foxm1* knockout human NPCs. These results suggest that *FOXM1*/*LIN28A* may increase the progenitor pool in mice in a similar manner. Overexpression of *Lin28a* increases Sonic hedgehog (Shh) in precursor cells by downregulating *let7*-miRNA

(Neumann *et al*, 2017). Constitutively active Sonic hedgehog (Shh) signaling increases the number of basal precursor cells and causes folding in mice (Wang *et al*, 2016). The expression of human *FOXM1* promotes cortical thickening and folding may be caused by activated Shh signaling via *LIN28A* downregulation of *let7*-miRNA, which will be studied in the future.

Taken together, our results highlight the function of human *FOXM1* in cortical expansion and folding in embryonic development. We find that *FOXM1* upregulates the expression of *Lin28a* by targeting the *Lin28a* promoter. The function of human *FOXM1* may provide new insights into the molecular mechanisms of cortical expansion and folding.

Materials and Methods

Animals

ICR(CD-1) pregnant mice obtained from Vital River Laboratories were used for all in utero electroporation experiments. The *hFOXM1*^{lox/+} mice were generated in the Experimental Animal Center of the Institute of Zoology, Chinese Academy of Sciences. Nestin-Cre mice were obtained from the Jackson Laboratory. The use of all mice in this study was conducted in accordance with the guidelines of the Animal Care and Use Committee of the Institute of Zoology, Chinese Academy of Sciences.

Human fetal brain collection

Human fetal brain tissues were collected at autopsy within 3 h of spontaneous abortion with the informed consent of the patients and in accordance with the Institute of Zoology, Chinese Academy of Sciences guidelines, and the study design was approved by the institutional review board (ethics committee) of the Institute of Zoology, Chinese Academy of Sciences. Brain tissues were stored in ice-cold Leibowitz-15 medium and transported to laboratory for further examination and processing.

FOXM1 conditional knock-in mouse construction

In brief, using CRISPR, sgRNA was inserted Rosa26 site between exon 1 and exon 2. Cas9 mRNA gRNA4 (CCGCGCGCCCTGC

GCAACGTGG) and donor DNA (CAGPr-loxP-stop- hFOXM1^{lox/+} mice were generated using gene editing technology based on CRISPR/Cas9 loxP-hFOXM1-3×flag-WPRE-PA flanked with 5'homologous arm/3'homologous arm) were microinjected into fertilized single-cell embryos. 569 zygotes were implanted into surrogate mothers. When mice were born, they were examined by tail genotyping. Only one was identified as *FOXM1*^{lox/+} mouse (F0). F0 mouse was bred with C57BL/6 mice. The offspring (F1) were confirmed by tail gene typing and PCR production sequencing. F1 mice were crossed with the Nestin-Cre mice, generating hFOXM1^{lox/+}; Nestin-Cre animals.

Plasmid constructs

293FT cell line RNA and fetal mouse brain (E15) RNA were reversed transcribed with Quant Script RT Kit (Tiangen). Human *FOXM1* cDNA was amplified by PCR and subcloned into the Xho1/BamH1 site of pCDH-copGFP vector. Mouse *Foxm1* cDNA was acquired by PCR and subcloned into the EcoR1/BamH1 site of pCDH-copGFP vector. The hFOXM1^{Δexon9} mutant plasmid was produced with Fast Site-Directed Mutagenesis Kit (Tiangen). Mouse *Foxm1*^{hexon9} mutant plasmid was acquired by nest PCR method. Human *LIN28A* cDNA was amplified by PCR and cloned the EcoR1/BamH1 site of pCDH-copGFP vector.

LIN28A/Lin28a-shRNA1/2/3 were cloned into the pSicoR-GFP vector. The sequences were as follows:

LIN28A/Lin28a-shRNA1: 5-CAAAGGAGACAGGTGCTACAA-3;
LIN28A/Lin28a-shRNA2: 5-CATCTGTAAGTGGTTCAACGT-3;
LIN28A/Lin28a-shRNA3: 5-CCAGCCCAAGAAGTGCCACTT-3.

In utero electroporation

The pregnant mice (ICR) were deeply narcotized with pentobarbital sodium, and the uterine horns were exposed. Plasmid DNA (> 1,500 ng/μl) mixed with 0.02% Fast Green(sigma) was microinjected into the fetal brain later ventricle, using a glass micropipette. Each fetal brain was electroporated for five 50 ms pulses at 40 V with 950-ms interval. After electroporation, the uterine horns were returned to the abdominal cavity. Then, the pregnant mouse was placed under the warm light until regaining activity.

Cell culture

Human embryonic kidney 293FT cell line and mouse neuroblastoma N2A cells (American Type Culture Collection) were used for transfection. Cells were cultured in DMEM (Gibco) supplemented with 10% FBS (Invitrogen) and 1% penicillin/streptomycin (Invitrogen).

Primary neural progenitor cells were isolated according to the protocol described previously (Xia *et al*, 2018). Briefly, E13 brain cortex was obtained under stereoscopic microscope and digested into cell suspension using 20 U/mg papain (Worthington). Cells were cultured on Poly-d-Lysine (Invitrogen) and Laminin (Invitrogen)-coated plates(costar) in proliferation medium composed of 50% DMEMF/12 medium (Gibco), 50% medium, 50 × B27 supplement without VA (Invitrogen), 100 × Gluta MAX (Invitrogen), 10 ng/ml EGF (Invitrogen), 10 ng/ml bFGF(Invitrogen), and 100× penicillin/streptomycin (Invitrogen).

H9 human embryonic stem cells (WiCell Research) were maintained on Matrigel-coated plates in DMEM essential 8 medium and 50× essential 8 supplements (Gibco). ES medium was replaced with fresh medium every day.

Generating human neural precursor cells

Generating NPC from human embryonic stem cell procedure was performed as described previously (Zhang *et al*, 2018). Briefly, when the growth density of human embryonic stem cells (ESCs) reaches 70%–80%, the ESCs medium was replaced with neural precursor cells differentiation medium. The medium was composed of 50% DMEMF/12 medium (Gibco), 50% medium, 50 × B27 supplement without VA (Invitrogen), 100 × Gluta MAX (Invitrogen), 10 ng/ml hLIF (Millipore), 2 μM dorsomorphin, 3 μM SB431542 (Tocris), 4 μM CHIR99021 (Stemgent), and 0.1 μM compound E (EMD Chemicals). After 5 days, cells dissociated into single cells with Accutase (Innovative Cell Technologies) were culture on Matrigel-coated plates in human neural precursor cell proliferation medium composed of 50% DMEMF/12 medium (Gibco), 50% medium, 50 × B27 supplement without VA (Invitrogen), 100 × Gluta MAX (Invitrogen), 10 ng/ml hLIF (Millipore), 2 μM SB431542, and 3 μM CHIR99021.

BrdU labeling, BrdU/EdU double labeling

For BrdU labeling, the pregnant mice were injected with 50 mg/kg BrdU (sigma) 2 h before embryonic brains were extracted and fixed at E15.

For BrdU/EdU double labeling, pregnant mice were injected with 50 mg/kg BrdU(sigma) at E14 and injected with 50 mg/kg EdU (sigma) 2 h before fetal brains were processed at E15.

Immunostaining and Western blotting

Brain slices and cultured cell immunostaining procedure were performed as described previously (Shen *et al*, 2018). In brief, brain slices fixed in 4% PFA for 30 min at room temperature and washed three times with PBS containing 1% Triton X-100 (1% PBST), each time for 10 min. The brain sections were blocked with 5% BSA (in 1% PBST) for 1 h at room temperature and then incubated with primary antibodies overnight at 4°C. Cultured cells were washed with PBS, fixed in 4% PFA for 20 min, washed three times with PBS including 0.1% Triton X-100 (0.1% PBST) for 10 min, blocked with 5% BSA (in 0.1% PBST) for 1 h at room temperature, then incubated with primary antibodies overnight at 4°C, and visualized after secondary antibodies for 1.5 h at room temperature.

For Western blotting, cells or brain tissues were lysed in RIPA lysis buffer containing protease inhibitor (1% cocktail and 1% PMSF). Protein samples were separated by 12% SDS–PAGE gel and transferred to polyvinylidene fluoride (PVDF) membranes. The PVDF membranes were blocked with 5% milk in PBST (PBS containing 0.02% Tween-20) for 1h at room temperature, then incubated with primary antibodies overnight at 4°C, and visualized after secondary antibodies for 1.5 h at room temperature.

Antibodies

The following primary antibodies and dilutions were used for immunostaining and Western blotting: anti-FOXM1 (ProteinTech, 13147-

1-AP; Rabbit, 1:1,000); anti-PAX6 (Millipore, AB2237; Rabbit, 1:1,000); anti-SOX2 (R&D, AF2018; Goat, 1:2,000); anti-SOX2 (Cell Signaling Technology, 3728s; Rabbit, 1:1,000); anti-BrdU (Abcam, AB6326; Rat, 1:1,000); anti-HOPX (ProteinTech, 11419-1-AP; Rabbit, 1:1,000); anti-P-VIM (Abcam, ab22651; Mouse, 1:1,000); anti-LIN28A (ProteinTech, 16177-1-AP; Rabbit, 1:1,000); anti-CTIP2 (Abcam, ab18465; Rat, 1:1,000); anti-SATB2 (Abcam, ab51502; Mouse, 1:500); anti- β -Actin (ProteinTech, 20536-1-AP; Rabbit, 1:10,000); anti- β -Actin (ProteinTech; 60008-1-Ig Mouse, 1:2,000); anti-Flag (Sigma, F7425; Mouse, 1:3,000); anti-PH3 (Cell Signaling Technology, 3377S; Rabbit, 1:1,000); anti-TUJ1 (Millipore, MAB1637; Rabbit, 1:2,000); Anti-GFAP (Dako, Z033429; Rabbit, 1:3,000); anti-ALDH1L1 (Abcam, ab56777; Rabbit, 1:500); anti-NeuN (Abcam ab177487; Rabbit, 1:1,000) anti-IgG (Bioss, bs-0295p; Rabbit, 1:1,000); anti-cleaved caspase 3 (Cell Signaling Technology, 9664S; Rabbit, 1:1,000); anti-caspase 3 (Cell Signaling Technology, 9662; Rabbit, 1:1,000).

The secondary fluorescence antibodies and dilutions for immunostaining are listed below: DAPI (2 mg/ml; Sigma; D9542); Alexa Fluor 488, Cy3, or Cy5 (Jackson ImmunoResearch, 1:1000) was used for nuclear counterstaining. The following secondary antibodies and dilutions were used for Western blotting: Donkey Anti-IgG (LI-COR Biosciences 800CW; Rabbit, 1:1,000); Donkey Anti-IgG (LI-COR Biosciences 800CW; Mouse, 1:1,000); Donkey anti-IgG (LI-COR Biosciences 680LT; Rabbit, 1:1,000); and Donkey anti-IgG (LI-COR Biosciences 680LT; Mouse, 1:1,000).

RT-PCR analysis

The total RNA from the hFOXM1 conditional knock-in mouse cerebral cortex or N2A cells was extracted by using the Fast Quant RT Kit (Tian gen). The analysis of real-time PCR was performed by using a SYBR qPCR master mix (Tian gen) and the ABI7500 real-time PCR system (Applied Biosystems). The primers used for real-time PCR were listed to Appendix Table S3.

RNA-sequencing analysis

Total RNA from E15 telencephalic tissue of WT and FOXM1-cKI mice was extracted. Specifically, Agilent 2100 Bioanalyze was used to quality controlled and quantified. Then, total RNA was converted to cDNA and bound to the library. RNA-sequencing analysis was used by the Illumina HiSeq 2500 platform in Annoroad Genomics.

Chromatin immunoprecipitation

Cells were treated with 1% fresh formaldehyde solution (fixing solution, 37% formaldehyde, PBS at a 0.7:0.3:10 ratio) for 10 min at room temperature. Then, 2.5 M glycine solution was added to each well for terminating the cross-linking reaction. Cells were washed twice with ice-cold PBS and resuspended in lysis buffer 1 (50 mM HEPES-KOH, pH = 7.5, 1 mM EDTA, 140 mM NaCl, 10% glycerol, 0.5% NP-40, 0.25% Triton, 1xPMSF, and 1x cocktail) for 10 min at 4°. Next, cells were washed with lysis buffer 2 (10 mM Tris-HCl, pH = 8.0, 200 mM NaCl, 1 mM EDTA, 0.5 mM EGTA, 1x PMSF, and 1x cocktail) for 10 min at 4°. After the cells were resuspended in lysis buffer 3 (10 mM Tris-HCl, pH = 8.0, 1 mM EDTA, 100 mM NaCl, 0.5 mM EGTA, 0.1% sodium deoxycholate, 1x

PMSF, and 1x cocktail), nuclei were sonicated by using a Scientz-IID sonicator. Lysates were incubated with anti-Flag-tag magnetic beads (Invitrogen) and anti-IgG magnetic beads (Invitrogen) overnight at 4°C. Beads were washed three times with low-salt buffer (0.1% SDS, 1% Triton X-100, 2mM EDTA, 150 mM NaCl, Tris-HCl, pH = 8.0) and three times with high-salt buffer (0.1% SDS, 1% Triton X-100, 2 mM EDTA, 500 mM NaCl, Tris-HCl, pH = 8.0) at room temperature. Immunocomplexes were eluted by using TES buffer (50 mM Tris-HCl pH 8.0, 10 mM EDTA, and 1% SDS) overnight at 65°. After extracted by DNA Gel Extraction Kit (Tiangen), DNA was used for RT-PCR. The primers used for real-time PCR were listed to Appendix Table S4.

Gyrification index analysis

The gyrification index (GI) is the ratio between the total outer cortical surface and the superficially exposed part of the outer surface (Zilles *et al*, 2013). We measured the local gyrification index (GI) that is a ratio of the local inner contour and outer contour at the same straight-line distance between two points. The cortex of frontal area and parietal area was measured. The width of 500 μ m was used for local GI measurements. All samples remain consistent.

Statistical analysis

All data analyses were performed using GraphPad Prism 6.0. Statistical analysis was performed using one-way ANOVA, or unpaired *t*-test. All results presented mean values \pm SEM.

Data availability

All data are available in the main manuscript or the Supplementary Materials. Transcriptome sequencing data are available in the Gene Expression Omnibus (GEO) repository under accession GSE145169 (<https://www.ncbi.nlm.nih.gov/geo/query/acc.cgi?acc=GSE145169>).

Expanded View for this article is available online.

Acknowledgements

We thank Z. Luo at School of Life Science and Technology in Shanghai Tech University for providing support for frozen sections of human tissue; S. Li, X. Zhu, and H. Qin for help with confocal imaging; and X. Lei, Q. Liang, Y. Li, and other members of the Jiao lab for helpful discussions. This work was supported by grants from the National Key R&D Program of China (2019YFA0110300, JJ), CAS Strategic Priority Research Program (XDA16010301), the National Science Fund for Distinguished Young Scholars (81825006, JJ), the National Natural Science Foundation of China (31730033 and 31621004, JJ), and Guangdong Natural Science Fund for Distinguished Young Scholars (2017A030306024, JZ).

Author contributions

WW and JJ designed the research; WW performed the research, drafted the manuscript, and analyzed data; LS and FJ contributed to image analysis and interpreted the data; DZ optimized the culture for human embryonic stem cells; YW, JZ, RDJ, MZ, EH, HJ, and JZ provided some advices about experiments; JJ supervised the project and acquired the funding support.

Conflict of interest

The authors declare that they have no conflict of interest.

References

- Chenn A, Walsh CA (2002) Regulation of cerebral cortical size by control of cell cycle exit in neural precursors. *Science* 297: 365–369
- Costa RH (2005) FoxM1 dances with mitosis. *Nat Cell Biol* 7: 108–110
- Dehay B (2014) Evidence piles Up for prion-like propagation mechanisms in synucleinopathies. *Mov Disord* 29: 187
- Dehay C, Kennedy H, Kosik KS (2015) The outer subventricular zone and primate-specific cortical complexification. *Neuron* 85: 683–694
- Deyama S, Li X-Y, Duman RS (2020) Neuron-specific deletion of VEGF or its receptor Flk-1 impairs recognition memory. *Eur Neuropsychopharmacol* 31: 145–151
- Fernandez V, Llinares-Benadero C, Borrell V (2016) Cerebral cortex expansion and folding: what have we learned? *EMBO J* 35: 1021–1044
- Fietz SA, Kelava I, Vogt J, Wilsch-Bräuninger M, Stenzel D, Fish JL, Corbeil D, Riehn A, Distler W, Nitsch R et al (2010) OSVZ progenitors of human and ferret neocortex are epithelial-like and expand by integrin signaling. *Nat Neurosci* 13: 690–699
- Fietz SA, Lachmann R, Brandl H, Kircher M, Samusik N, Schroder R, Lakshmanaperumal N, Henry I, Vogt J, Riehn A et al (2012) Transcriptomes of germinal zones of human and mouse fetal neocortex suggest a role of extracellular matrix in progenitor self-renewal. *Proc Natl Acad Sci USA* 109: 11836–11841
- Florio M, Albert M, Taverna E, Namba T, Brandl H, Lewitus E, Haffner C, Sykes A, Wong FK, Peters J et al (2015) Human-specific gene ARHGAP11B promotes basal progenitor amplification and neocortex expansion. *Science* 347: 1465–1470
- Florio M, Heide M, Pinson A, Brandl H, Albert M, Winkler S, Wimberger P, Huttner WB, Hiller M (2018) Evolution and cell-type specificity of human-specific genes preferentially expressed in progenitors of fetal neocortex. *Elife* 7: e32332
- Groszer M, Erickson R, Scripture-Adams DD, Dougherty JD, Le Belle J, Zack JA, Geschwind DH, Liu X, Kornblum HI, Wu H (2006) PTEN negatively regulates neural stem cell self-renewal by modulating G0–G1 cell cycle entry. *PNAS* 103: 111–116
- Hansen DV, Lui JH, Parker PR, Kriegstein AR (2010) Neurogenic radial glia in the outer subventricular zone of human neocortex. *Nature* 464: 554–561
- Herrlinger S, Shao Q, Yang M, Chang Q, Liu Y, Pan X, Yin H, Xie LW, Chen JF (2019) Lin28-mediated temporal promotion of protein synthesis is crucial for neural progenitor cell maintenance and brain development in mice. *Development* 146: dev173765
- Hou Q-Q, Xiao Q, Sun X-Y, Ju X-C, Luo Z-G (2021) TBC1D3 promotes neural progenitor proliferation by Ga9. *Sci Adv* 7: eaba8053
- Hu C, Liu D, Zhang Y, Lou G, Huang G, Chen B, Shen X, Gao M, Gong W, Zhou P et al (2014) LXRalpha-mediated downregulation of FOXM1 suppresses the proliferation of hepatocellular carcinoma cells. *Oncogene* 33: 2888–2897
- Johnson TC (1994) Negative regulators of cell proliferation. *Pharmacol Ther* 62: 247–265
- Laoukili J, Stahl M, Medema RH (2007) FoxM1: at the crossroads of ageing and cancer. *Biochim Biophys Acta* 1775: 92–102
- Liu J, Liu W, Yang LU, Wu Q, Zhang H, Fang AI, Li L, Xu X, Sun LE, Zhang J et al (2017) The primate-specific gene TMEM14B marks outer radial glia cells and promotes cortical expansion and folding. *Cell Stem Cell* 21: 635–649
- Lui JH, Hansen DV, Kriegstein AR (2011) Development and evolution of the human neocortex. *Cell* 146: 18–36
- Miller JA, Ding S-L, Sunkin SM, Smith KA, Ng L, Szafer A, Ebbert A, Riley ZL, Royall JJ, Aiona K et al (2014) Transcriptional landscape of the prenatal human brain. *Nature* 508: 199–206
- Miyazawa H, Muramatsu Y, Makino H, Yamaguchi Y, Miura M (2019) Temporal regulation of Lin28a during mammalian neurulation contributes to neonatal body size control. *Dev Dyn* 248: 931–941
- Neumann JE, Wefers AK, Lambo S, Bianchi E, Bockstaller M, Dorostkar MM, Meister V, Schindler P, Korshunov A, von Hoff K et al (2017) A mouse model for embryonal tumors with multilayered rosettes uncovers the therapeutic potential of Sonic-hedgehog inhibitors. *Nat Med* 23: 1191–1202
- Nonaka-Kinoshita M, Reillo I, Artegiani B, Martinez-Martinez MA, Nelson M, Borrell V, Calegari F (2013) Regulation of cerebral cortex size and folding by expansion of basal progenitors. *EMBO J* 32: 1817–1828
- Ostrem B, Di Lullo E, Kriegstein A (2017) oRGs and mitotic somal translocation - a role in development and disease. *Curr Opin Neurobiol* 42: 61–67
- Pillay P, Manger PR (2007) Order-specific quantitative patterns of cortical gyrification. *Eur J Neurosci* 25: 2705–2712
- Pollen A, Nowakowski T, Chen J, Retallack H, Sandoval-Espinosa C, Nicholas C, Shuga J, Liu S, Oldham M, Diaz A et al (2015) Molecular identity of human outer radial glia during cortical development. *Cell* 163: 55–67
- Reillo I, Borrell V (2012) Germinal zones in the developing cerebral cortex of ferret: ontogeny, cell cycle kinetics, and diversity of progenitors. *Cereb Cortex* 22: 2039–2054
- Reillo I, de Juan RC, Garcia-Cabezas MA, Borrell V (2011) A role for intermediate radial glia in the tangential expansion of the mammalian cerebral cortex. *Cereb Cortex* 21: 1674–1694
- Shen T, Ji F, Wang Y, Lei X, Zhang D, Jiao J (2018) Brain-specific deletion of histone variant H2A.z results in cortical neurogenesis defects and neurodevelopmental disorder. *Nucleic Acids Res* 46: 2290–2307
- Shyh-Chang N, Daley GQ (2013) Lin28: primal regulator of growth and metabolism in stem cells. *Cell Stem Cell* 12: 395–406
- Sun T, Hevner RF (2014) Growth and folding of the mammalian cerebral cortex: from molecules to malformations. *Nat Rev Neurosci* 15: 217–232
- Wang L, Hou S, Han YG (2016) Hedgehog signaling promotes basal progenitor expansion and the growth and folding of the neocortex. *Nat Neurosci* 19: 888–896
- Wierstra I, Alves J (2007) FOXM1, a typical proliferation-associated transcription factor. *Biol Chem* 388: 1257–1274
- Wong FK, Marin O (2019) Developmental cell death in the cerebral cortex. *Annu Rev Cell Dev Biol* 35: 523–542
- Xia W, Su L, Jiao J (2018) Cold-induced protein RBM3 orchestrates neurogenesis via modulating Yap mRNA stability in cold stress. *J Cell Biol* 217: 3464–3479
- Zhang N, Wei P, Gong A, Chiu WT, Lee HT, Colman H, Huang H, Xue J, Liu M, Wang Y et al (2011) FoxM1 promotes beta-catenin nuclear localization and controls Wnt target-gene expression and glioma tumorigenesis. *Cancer Cell* 20: 427–442
- Zhang W, Wan H, Feng G, Qu J, Wang J, Jing Y, Ren R, Liu Z, Zhang L, Chen Z et al (2018) SIRT6 deficiency results in developmental retardation in cynomolgus monkeys. *Nature* 560: 661–665
- Zilles K, Palomero-Gallagher N, Amunts K (2013) Development of cortical folding during evolution and ontogeny. *Trends Neurosci* 36: 275–284